Carbohydrate Polymers 86 (2011) 1291–1299

Contents lists available at ScienceDirect

Carbohydrate Polymers

journal homepage: www.elsevier.com/locate/carbpol

Isolation of nanocellulose from waste sugarcane bagasse (SCB) and its characterization

Arup Mandal, Debabrata Chakrabarty*

Department of Polymer Science and Technology, Calcutta University, 92 Acharya Prafulla Chandra Road, Kolkata 700 009, India

ARTICLE INFO

Article history:
Received 27 April 2011
Received in revised form 9 June 2011
Accepted 13 June 2011
Available online 16 July 2011

Keywords:
Sugarcane bagasse
Nanocellulose
Thermoresistant
DLS
AFM

ABSTRACT

Nanocellulose obtained by acid hydrolysis of sugarcane bagasse (SCB) has been characterized by Fourier transformed infrared (FTIR) spectra, thermogravimetric analysis (TGA), differential scanning calorimetry (DSC), X-ray diffraction (XRD), dynamic light scattering (DLS), scanning electron microscopy (SEM) and atomic force microscopy (AFM) and transmission electron microscopy (TEM) studies. Nanocellulose and cellulose exhibited identical FTIR spectra quite different from SCB. TG analysis shows that the bagasse starts to degrade earlier than cellulose and the nanocellulose shows an even earlier onset of degradation compared to SCB but leaves the maximum residue within the range of temperatures studied. DSC studies revealed that SCB, cellulose and the nanocellulose differ in their loosely bound moisture content. The nanocellulose exhibits an intermediate behavior between SCB and cellulose. The XRD shows enrichment in the proportion of crystalline cellulose in nanocellulose, which manifests significant conversion of cellulose I to cellulose II. DLS studies show particle size distribution in the nanorange which has been substantiated by SEM, AFM and TEM.

1. Introduction

Cellulose, the major constituent of all plant materials including wood, cotton, flax, hemp, jute, ramie, cereal straws, rice straws and sugarcane bagasse, forms about half to one-third of plant tissues and is constantly replenished by photosynthesis. Thus it is the most abundant and renewable natural resource on earth (Goodger, 1976).

Sugarcane bagasse is a residue produced in large quantities every year by the sugar and alcohol industries, and is mainly used as a fuel to power the sugar mill (Simkovic, Mlynar, & Alfoldi, 1990). Several processes and products have been reported that utilize bagasse as a raw material for industrial applications. These include electricity generation, pulp and paper production, and products based on fermentation (Pandey, Soccol, Nigam, & Soccol, 2000). The utilization of this biomass for processing of novel composites has attracted growing interest because of their ecological and renewable characteristic (Cherian et al., 2010).

In the present investigation bagasse has been used for the production of microcrystalline cellulose and nanocellulose. About 40–50% of bagasse is the glucose polymer cellulose, much of which is in crystalline structure. Another 25–35% is hemicellulose, an amorphous polymer usually composed of xylose, arabinose, galactose, and mannose. The remainder is mostly lignin (18–24%); plus lesser amounts of mineral, wax (<1%), and ash (1–4%) (Jacobsen & Wyman, 2002; Wyman, 1999). Normally it contains moisture to the extent of 40–50%. Chemically, cellulose is a linear, stereoregular natural homopolymer composed of anhydroglucose units linked at one and four carbon atoms by β-glycosidic bonds. This is confirmed by the presence of three hydroxyl groups (secondary OH at the C-2, and at the C-3 and primary OH at the C-6 position) with different reactivities (Kadla & Gilbert, 2000). These hydroxyl groups and their ability to form hydrogen bonds play a major role in directing the crystal packing and also governing the physical properties of cellulose. In cellulosic plant fiber, cellulose is present in an amorphous state, but also associated with crystalline phases through both intermolecular and intramolecular hydrogen bonding for which cellulose does not melt before thermal degradation (Fengel & Wegner, 1989; Klemm, Heublein, Fink, & Bohn, 2005). Cellulose is organized into fibrils, which are aligned parallel to each other, surrounded by a matrix of lignin and hemicelluloses. The properties of cellulose including good mechanical properties, low density, and biodegradability (Zimmerman, Pöhler, & Schwaller, 2005) depend on the type of cellulose present. There are several types of celluloses (I, II, III, IV, and V) and type I shows the best mechanical properties. At present, it seems generally accepted that cellulose I has a parallel chain orientation, while in cellulose II, the chains are anti-parallel (Lennholm & Iversen, 1995).

Cellulose nanoparticles have been synthesized in spherical form (Pu et al., 2007; Zhang, Jiang, Dang, Elder, & Ragauska, 2008),

* Corresponding author. Tel.: +91 9830773792.
E-mail address: chakrabarty_deb@yahoo.com (D. Chakrabarty).

0144-8617/$ – see front matter © 2011 Elsevier Ltd. All rights reserved.
doi:10.1016/j.carbpol.2011.06.030

rod-like highly crystalline nanocrystals (Azizi-Samir, Alloin, & Dufresne, 2005; Dufresne, 2006, 2008; Lima & Borsali, 2004) which are obtained by acid hydrolysis of cellulosic fibers, and microfibrillated cellulose (MFC) resulting from disintegration of cellulose fibers under high shearing and impact forces (Teixeira et al., 2009).

In this work, we obtained nanocellulose from the most abundant, inexpensive, and readily available lignocellulosic material such as sugarcane bagasse by the hydrolysis of delignified, hemicellulose free cellulose with a strong acid such as sulfuric acid (Bondeson, Mathew, & Oksman, 2006; Nickerson & Habrle, 1947; Ranby, 1952). Nanocellulose from acid hydrolysis of microcrystalline cellulose typically has a wide range in size.

Geometrical characteristics of nanocellulose depend on the hydrolysis conditions such as temperature and time (Dong, Revol, & Gray, 1998), and the original source of cellulose fibers: e.g., bacterial cellulose (Grunert & Winter, 2000, 2002), cotton filter paper (Dong et al., 1998; Edgar & Gray, 2002), and tunicates (Heux, Chauve, & Bonini, 2000). It is known from the literature that the nanocellulose from other conventional sources exhibits high stiffness and Young's modulus which goes sometimes as high as 134 GPa (Oksmann & Sain, 2006). The tensile strength of the crystal structure is assumed to be approximately 0.8 up to 10 GPa (Nishino, Takano, & Nakamae, 1995). Here an attempt has been made to synthesize nanocellulose from the bagasse and compare its properties with the values obtained so far from other conventional resources. This also offers an opportunity to the effective disposal of the waste.

Controlled acid hydrolysis of native cellulose fibers disrupts the fibers which can then be dispersed into their constituent rod-shaped elementary crystalline microfibrils. Colloidal suspensions of these rods are known to exhibit birefringence and ordered liquid crystalline phases (Araki, Wada, Kuga, & Okano, 2000; Dong et al., 1998; Marchessault, Morehead, & Walter, 1959; Orts, Godbout, Marchessault, & Revol, 1998; Revol et al., 1994).

The use of acid hydrolysis to reduce cellulose crystallinity has been adopted by many researchers (El-sakhawy & Hassan, 2007; Sidiras & Koukios, 1989; Sun, Sun, Zhao, & Sun, 2004). Basically, strong acids are oxidizing agents and would dehydrate and redistribute the biopolymers in lignocellulosic materials (Song & Lee, 1984). The effect of acid hydrolysis on the crystallinity of cellulose is also studied and their results showed that, with an increase in acid concentrations, the crystallinity index decreased rapidly. In addition, the presence of sodium hydroxide decreased the crystallinity index of α-cellulose because sodium hydroxide penetrates and swells the cellulose fiber (Rozmarin et al., 1977).

There are a great number of potential applications of nanocellulose within different industries, viz. high quality paper products; in cosmetics as thickener and in food industry as stabilizer, fat replacer and texturing agent; moldable light weight, high strength materials; composites for construction, vehicles, customer products, furnitures; new materials for electronics and pharmaceutical applications. Industrial grades microcrystalline cellulose has a high proportion of sub-micron size colloidal microcrystals which are excellent stabilizing agents for water based latex paints as well as for industrial coating and suspensions (Janovsky, McCredia, & Janet, 1995; Ono & Keiko, 1995; Panosyan, Skurikhin, Sviridov, & Kiseleva, 1994).

2. Experimental

2.1. Materials

Locally available lignocellulosic material such as sugarcane bagasse was collected, sorted and cleaned. Bagasse was depithed manually. It was first dried in sunlight and then cut into small pieces (1–3 cm). The cut bagasse was grinded and the fraction passing through 60 mesh (less than 0.250 mm size screen) was selected for subsequent extraction of cellulose. The ground bagasse was further dried in a hot air oven for 16 h at 60 °C.

Other reagents used were: sodium chlorite (Loba Chemie, India); acetic acid (Merck, India); buffer solution (Merck, India); sodium sulfite (Merck, India); sodium hydroxide (Merck, India); acetone (International Chemicals, India); dimethylsulfoxide (Merck, India); sulfuric acid (Merck, India). All the chemicals were reagent grade and were used as received.

2.2. Methods

2.2.1. Delignification of cellulose from bagasse

The dried and ground bagasse was first bleached with 0.7% (w/v) sodium chlorite solution (fiber to liquor ratio of 1:50) at pH 4, adjusted by 5% acetic acid and maintained with buffer solution of pH 4 while the mixture was being boiled for 5 h to remove the lignin. The residue was subsequently washed with distilled water. This neutral residue was then boiled with 250 ml 5% (w/v) sodium sulfite solution for 5 h, followed by washing with adequate distilled water to remove the lignin completely and hemicellulose partially.

2.2.2. Isolation of cellulose

The holocellulose thus obtained was boiled with 250 ml 17.5% (w/v) sodium hydroxide solution for 5 h to remove the hemicelluloses. At the end of the extraction, the insoluble residue (cellulose) was collected by filtration through Micro Filter Holder Assembly (MFHA) and washed thoroughly with distilled water until the filtrate was neutral. The resulting cellulosic materials were air-dried, and then added to 50 ml dimethylsulfoxide (DMSO) in an 80 °C water bath for 3 h. The product thus obtained was then filtered, washed with distilled water and air-dried.

2.2.3. Preparation of nanocellulose

An aqueous suspension of nanocellulose was prepared as follows. The delignified and hemicellulose free cellulose, as obtained earlier was acid hydrolyzed by refluxing with 60% (w/v) sulfuric acid (fiber to liquor ratio of 1:20) for 5 h at 50 °C under strong agitation. The hydrolysis was quenched by adding 5-fold excess water (100 ml) to the reaction mixture. The resulting mixture was cooled to room temperature and centrifuged. The fractions were continuously washed by the addition of distilled water and centrifuged. The centrifugation process was stopped after at least five washings, while the supernatant liquor became turbid, i.e., becoming a colloidal suspension. Under this condition, the pH of the suspension was above 5. The suspension was then sonicated (UP-500 Ultrasonic Processor with Probe) for 5 min in an ice bath to avoid overheating, which can cause desulfation of the sulfate groups on the cellulose (Dong et al., 1998). The newly generated suspension was stored in refrigerator at 4 °C.

3. Characterization methods

3.1. Fourier transform infrared (FTIR) spectroscopy

The FTIR spectra of the cellulosic samples were recorded on an instrument (Shimadzu FTIR 8400) in the range of 500–4500 cm^{-1} with a resolution of 4 cm^{-1}. The samples were ground into powder by a fiber microtome and then blended with KBr followed by pressing the mixture into ultra-thin pellets.

3.2. Thermal analyses

3.2.1. Thermogravimetric analysis (TGA)

A Pyris 1 Thermal Gravimetric Analyzer (Pyris Diamond TGA, Perkin-Elmer, USA) was used to characterize the thermal stability

of the cellulose samples. Approximately 2 mg of each sample was heated from 30 °C to 750 °C at a heating rate of 10 °C/min. All of the measurements were performed under a nitrogen atmosphere with a gas flow of 20 ml/min in order to prevent any thermoxidative degradation.

3.2.2. Differential scanning calorimetry (DSC)

Using a DSC-60 differential scanning calorimeter (Shimadzu D 60), the thermal behavior of the cellulose samples was studied. Each sample was heated from 30 °C to 350 °C at a heating rate of 10 °C under nitrogen atmosphere. The thermograms were used to determine the onset melting temperature and crystallization temperature.

3.3. X-ray diffraction (XRD)

Wide-angle X-ray diffraction data were collected using a Rigaku Miniflex X-ray diffractometer equipped with Cu Kα radiation at 30 kV and 15 mA to investigate the XRD spectra of the cellulosic sample. Scattered radiation was detected in the range $2\theta = 5–50°$, at a speed of 3°/min.

3.4. Measuring the particle size by dynamic light scattering (DLS) test

Particle size was measured by laser diffractometry using a Nano Size Particle Analyzer (ZEN 1600 MALVERN USA) in the range between 0.6 nm and 6.0 μm, under the following conditions: particle refractive index 1.59, particle absorption coefficient 0.01, water refractive index 1.33, viscosity 0.8872 cP, temperature 25 °C and general calculation model for irregular particles. Thirteen measurement cycles of 10 s each were taken and the average was done using software (DTS, Ver. 5.00 from Malvern).

3.5. Microscopic analyses

3.5.1. Scanning electron microscopy (SEM)

Scanning electron microscopy (SEM) photographs of virgin sugarcane bagasse and treated fibers surfaces were captured using Hitachi SEM S3400N (Japan). In this case, the samples were coated with gold using the sputtering technique.

3.5.2. Atomic force microscopy (AFM)

AFM was used to characterize the morphology or the dimensional image of cellulose fibers obtained from acid hydrolyzed alkali treated sugarcane bagasse. Measurements were performed in tapping mode by a Veeco Nanoscope IIIa atomic force microscope (USA) at ambient temperature. In the sample preparation, a drop of diluted aqueous suspension (sonicated) of cellulose fibers was dispersed on the surface of an optical glass substrate and allowed to dry at ambient temperature and analyzed subsequently.

3.5.3. Transmission electron microscopy (TEM)

About 10 μl drop of dilute suspension of nanocellulose was given on a carbon coated Cu grid, it was then dried under table lamp and then stained for 3 min with Ruthenium vapor. Transmission electron micrographs (TEM) images were obtained using a TECNAI T12 FEI transmission electron microscope (Germany) with an acceleration voltage of 120 kV.

4. Results and discussion

4.1. Role of special chemical agents in the process of extraction on the properties of cellulose and nanocellulose

The role of sodium sulfite in the process of delignification of cellulose is to absorb the lignin–chlorine complex formed during the process of digestion of bagasse with sodium chlorite. This lignin–chlorine complex is highly soluble in sodium sulfite solution. At the same time it has been reported that hemicellulose can also be removed to some extent by boiling with sodium sulfite solution (Norman and Jenkins, 1933).

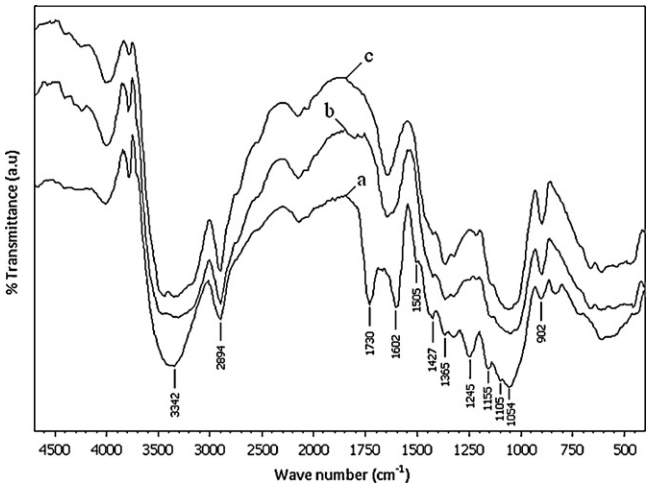

Fig. 1. FTIR spectra of (a) untreated sugarcane bagasse; (b) alkali treated bagasse, i.e., cellulose; and (c) acid hydrolyzed cellulose, i.e., nanocellulose.

The purpose of DMSO treatment after the removal of hemicellulose during the synthesis of pure cellulose mainly is to swell the cellulose so that the hydrolyst (sulfuric acid) can diffuse into the fibers more easily, during the subsequent acid hydrolysis step.

Treating the 'lignin and hemicellulose free' cellulose with sulfuric acid involves esterification of hydroxyl groups, besides the hydrolysis of the glycosidic linkages rendering extensive reduction in DP and particle size consequently (Yao, 1999). However, the introduction of sulfate groups along the surface of the cellulose crystallites will result in a negative charge on the surface. This anionic stabilization via the attraction/repulsion forces of the electrical double layers at the crystallites is probably the reason for the stability of the colloidal suspensions of the so-called nanocellulose crystallites (Marchessault, Morehead, & Koch, 1961). However, upon drying, the crystalline fragments became rod-like and aggregated to some extent. The aggregation might have resulted from the formation of hydrogen bonds through the hydroxyl groups and the high surface energy of the cellulose nanofibers.

4.2. FTIR spectroscopy analysis

FTIR spectroscopy has been extensively used in cellulose research, since it presents a relatively easy method of obtaining direct information on chemical changes that occur during various chemical treatments (Ristolainen, Alen, Malkavaara, & Pere, 2002).

In the FTIR analysis, the spectra of sugar cane bagasse, alkali treated bagasse, i.e., cellulose and the sulfuric acid hydrolyzed cellulose, i.e., nanocellulose are shown in Fig. 1.

The peak centered at 1730 cm^{-1} in the FTIR spectrum of ground sugarcane bagasse is predominantly attributed to the C=O stretching vibration of the acetyl and uronic ester groups, from pectin, hemicellulose or the ester linkage of carboxylic group of ferulic and p-coumaric acids of lignin and/or hemicellulose (Sain & Panthapulakkal, 2006; Sun, Xu, Sun, Fowler, & Baird, 2005). Likewise, the absorption peaks at 1602 cm^{-1} and faintly at 1505 cm^{-1} are associated with the aromatic C=C in plane symmetrical stretching vibration of aromatic ring present in lignin (Garside & Wyeth, 2003; Wang et al., 2009). The peak at 1245 cm^{-1} as present only in spectra of bagasse stands for the C–O out of plane stretching vibration of the aryl group in lignin (Troedec et al., 2008). All these have

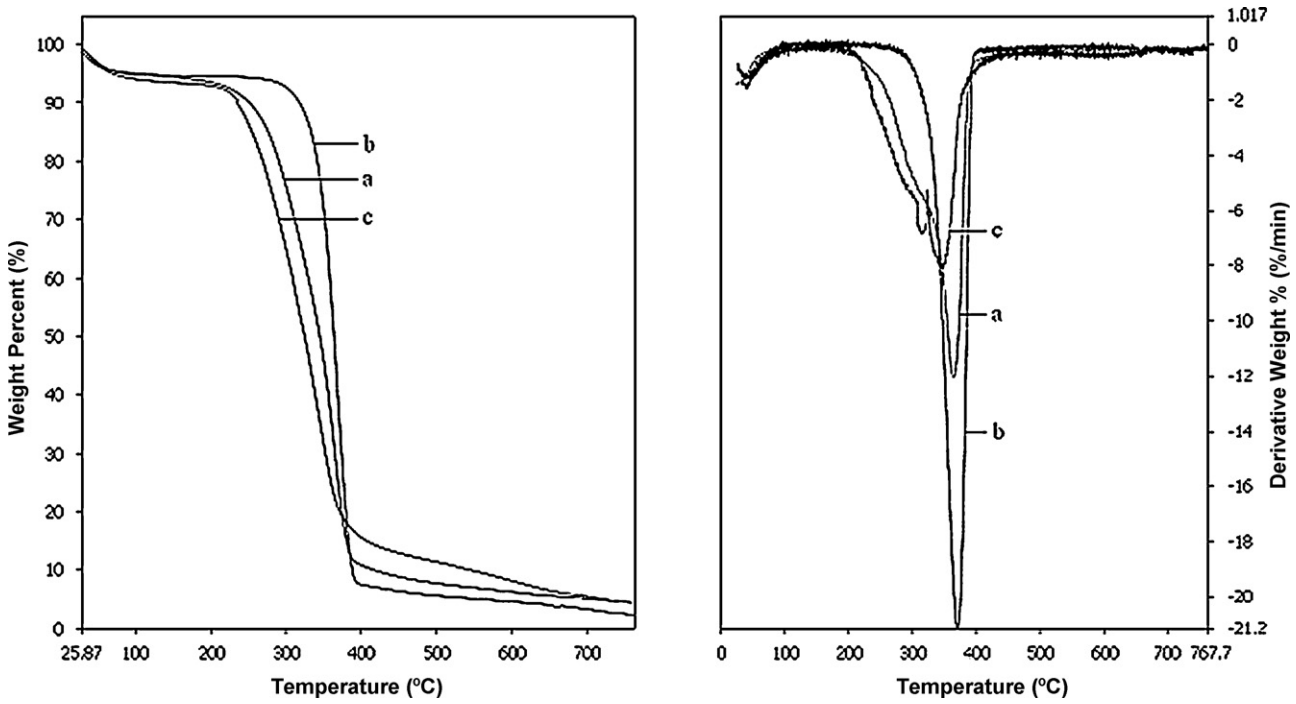

Fig. 2. TG and DTG curve of (a) untreated sugarcane bagasse; (b) alkali treated bagasse, i.e., cellulose; and (c) acid hydrolyzed cellulose, i.e., nanocellulose.

disappeared completely in the spectra of cellulose fibers obtained after $NaClO_2$ treatment and alkali treatment. These peaks are also absent in the sulfuric acid hydrolyzed cellulose (nanocellulose). The spectrum of nanocellulose, however, resembles that of cellulose obtained after alkali treatment.

The FTIR spectra of the untreated and treated sugarcane bagasse have exhibited a broad band in the region 3500–3200 cm^{-1} that indicates the free O–H stretching vibration of the OH groups in cellulose molecules. Moreover, the spectra of all samples showed the characteristic C–H stretching vibration around 2894 cm^{-1} (Khalil et al., 2001). In addition, the vibration peak detected at 1365 cm^{-1} in all samples has been related to the bending vibration of the C–H and C–O bonds in the polysaccharide aromatic rings (Nacos et al., 2006; Troedec et al., 2008). Besides, the absorbance peaks observed in the spectra of cellulose fibers obtained after alkali treatment and the nanocellulose in the region 1649–1641 cm^{-1} are attributed to the O–H bending of the adsorbed water (Troedec et al., 2008).

The peak observed in the spectra of all samples at 1054 cm^{-1} is due to the C–O–C pyranose ring (antisymmetric in phase ring) stretching vibration. The most significant absorption band which continually increases on alkaline and acid hydrolysis, respectively, of sugarcane bagasse is that of 902 cm^{-1} (associated with the β-glycosidic linkages between glucose units in cellulose) which stands for cellulose II, the content of which increases progressively from bagasse to nanocellulose (Pappas, Tarantilis, Daliani, Mavromoustakos, & Polissiou, 1999).

The C–C ring breathing band at ~1155 cm^{-1} and the C–O–C glycosidic ether band at 1105 cm^{-1} both of which arise from the polysaccharide component is getting gradually lost in nanocellulose because of hydrolysis and reduction in molecular weight (Garside & Wyeth, 2003).

4.3. Thermal analyses

4.3.1. Thermogravimetric analysis (TGA)

TG and DTG curves of sugarcane bagasse, pure cellulose derived from bagasse (after removal of lignin and hemicellulose) and the acid hydrolyzed cellulose from bagasse (i.e., nanocellulose) are shown in Fig. 2. The initial weight losses starting at ~26 °C for both the native ground bagasse and the alkali treated lignin free bagasse, i.e., pure cellulose and at 30 °C for the sulfuric acid hydrolyzed bagasse (after initial treatment with $NaClO_2$ followed by alkali digestion) may be attributed to the evaporation of loosely bound moisture on the surfaces of these materials. The chemisorbed water or the intermolecularly H-bonded water (as apparent from the characteristic peak of FTIR spectra at 1649 or 1641 cm^{-1}) is found to be given off at 120 °C for almost all the three varieties of cellulose as obtained after different modes of treatment.

In the case of acid hydrolyzed bagasse sample the increased portion of moisture (5.76%) with respect to bagasse may be assumed to be due to the higher extent of solvation or ionic association around the sulfated cellulose molecules by the water molecules. The sulfated amorphous region in case of nanocellulose may also provide for enhanced interchain spaces where moisture can get entrapped. The marginally higher moisture content in case of cellulose might be ascribed to the absorption of moisture in the spaces left vacant on the removal of hemicellulose and lignin to some extent. It is the more open surface created in alkali treated cellulose which helps to absorb moisture relatively more than that of the bagasse.

It is quite interesting to note that, while the degradation of bagasse and the alkali treated bagasse follow almost identical mechanism, the degradation of the acid hydrolyzed nanocellulose is associated with an additional small hump or shoulder around 311 °C. The degradation of untreated bagasse ensues at 273 °C and the rate of degradation reaching its peak at 363 °C (revealed by DTG curve) while that of the alkali treated cellulose occurs at 343 °C and the rate of degradation becoming maximum at 370 °C (revealed by DTG curve). The acid hydrolyzed specimen of nanocellulose sets to degradation at 249 °C and the peak rate of degradation is reached at 345 °C (also revealed by DTG curve). It can be anticipated that the presence of hemicellulose, lignin and other non-cellulosic constituents which decompose at low temperatures help to cause early onset of degradation of the bagasse. In the alkali treated bagasse, i.e., pure cellulose, however, the removal of all these non-cellulosic materials helps to make the cellulose structure more dense and compact and hence the rise in the onset temperature of

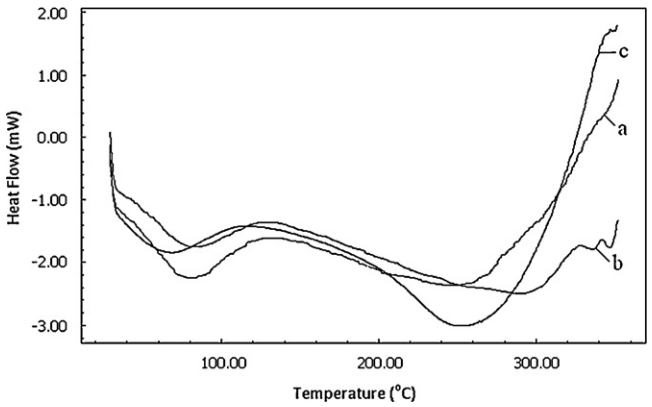

Fig. 3. DSC curve of (a) untreated sugarcane bagasse; (b) alkali treated bagasse, i.e., cellulose; and (c) acid hydrolyzed cellulose, i.e., nanocellulose.

degradation. The rearrangement and reorientation of the crystals in cellulose offers to raise the onset temperature of degradation. In the case of acid hydrolyzed bagasse we find somewhat reduction in the early onset temperature of degradation with respect to both the native cellulose from bagasse and the cellulose obtained after its alkali treatment. The lower initial temperature of decomposition at 249 °C and the broader degradation range of nanocellulose may correspond to the drastic reduction in molecular weight and degradation of more accessible and therefore more highly sulfated amorphous regions (present only in case of acid hydrolyzed specimen) in particular. The degradation of acid hydrolyzed alkali treated bagasse appears to follow a different mechanism and this is manifested by the presence of two humps in close proximity (Maren & William, 2004). The lower temperature stage showing a peak at around 311 °C (quite apparent in the DTG curve) may correspond to the degradation of more accessible and therefore more highly sulfated amorphous regions, whereas the higher temperature stage showing a peak at around 345 °C is related to the breakdown of unsulfated crystal interior. Actually the introduction of sulfated groups into the crystals of cellulose in the sulfuric acid hydrolysis process thus reduces the thermal stability of the product (Julien, Chornet, & Overend, 1993; Kim, Nishiyama, Wad, & Kuga, 2001).

The bagasse, the cellulose and the consequent nanocellulose extracted out of it, all undergo a two-step degradation process. In case of untreated bagasse the second step is initiated at 381 °C while those of cellulose and nanocellulose are initiated at 385 °C and 373 °C, respectively. The order of initiation in the second step follows the sequence similar to that of the first step. The residues remaining from the previous step of degradation at this onset temperature of degradation stand as 10.63% for bagasse, 7.68% for cellulose and 15.58% for nanocellulose. In spite of the losses in weight of the low temperature degrading non-cellulosic constituents (lignin and hemicellulose), the high percentage of bagasse residue at the end of the first step of degradation, with respect to the cellulose (Nguyen, Zavarin, & Barrall, 1981) is probably due to the presence of more amount of crystalline cellulose I having parallel orientation. The cellulose before acid hydrolysis contains more of less crystalline cellulose II (having antiparallel orientation) and amorphous cellulose. The further increase in percentage remnant in case of nanocellulose after the first step of degradation can be ascribed to sulfated amorphous and crystalline regions of cellulose which are intrinsically flame resistant (Maren & William, 2004).

4.3.2. Differential scanning calorimetry (DSC)

Fig. 3 shows the DSC diagrams of raw bagasse, pure cellulose and nanocellulose. All the three DSC thermograms exhibit two distinct endothermic changes within the range of temperature studied. The nature of endotherms, however, is quite characteristic of the composition of the material and differs from each other.

The initial endotherm which occurs in all the three cases at temperature much lower than 100 °C stands for the loss of moisture due to evaporation. Such type of moisture loss is also corroborated by the TGA studies. Both the bagasse and the pure cellulose display almost similar onset temperature of moisture loss while the former exhibits a higher final temperature for the process. Bagasse consists of hemicellulose, lignin and other non-cellulosic constituents besides the cellulose itself. All these hydrophilic substances help to retain moisture not only in greater proportion but also cause the variation in the sorptive forces holding this moisture. This possibly explains why the process of moisture loss occurs over a wide range of temperature. The chemically treated bagasse (after sequential treatment with sodium chlorite and caustic solution) may be assumed to contain no hemicellulose and lignin. Thus the apparently pure cellulose might have adsorbed moisture with a relatively uniform sorptive forces and thus causing the moisture loss within a reasonably narrower range of temperature.

The course of moisture loss in case of cellulose and acid (sulfuric acid) hydrolyzed bagasse, i.e., the so-called nanocellulose is quite noteworthy. Firstly, the sulfuric acid acts as a dehydrating catalyst. Secondly on acid hydrolysis of the alkali treated bagasse, i.e., the cellulose crystals particularly on its active surfaces get sulfated, a phenomenon which remarkably reduces the affinity for moisture absorption. Though some small quantity of moisture gets adsorbed on its surfaces, it is, however, loosely bound and gets evaporated off at much lower temperature.

The second endotherm in each of the three cases is an indication of the course of fusion or melting which gives an idea of the nature of decomposition of the crystallites, the extent of which gradually increase in going from bagasse to nanocellulose, the nature of amorphous regions and the influences of the non-cellulosic constituents during the fusion process.

In the case of ground bagasse, we observe the fusion process occurring over a wide range of temperature (161–241 °C). Ground bagasse is supposed to contain varying proportion of non-cellulosic constituents like hemicellulose, lignin, pectin, etc. besides the major cellulose. All these materials have their own characteristic melting region and a confluence of all these is reflected in the nature and width of the present endotherm.

The bagasse on treatment with sodium chlorite and subsequently with alkali is supposed to loose a substantial proportion of the non-cellulosic materials and in this process the cellulose crystals get rearranged and reoriented leading to a more compact crystal structure. This causes not only a higher onset of crystalline melting temperature but also a narrow endotherm width in turn (253–290 °C). The pure cellulose thus exhibits the DSC pattern within the temperature range under investigation with its characteristic endotherm.

The alkali treated bagasse on further hydrolysis in a sulfuric acid medium undergoes remarkable changes in their ultimate crystal structure, size of particles, etc. The accessible hydroxyl groups as present in alkali treated bagasse (pure cellulose) are now sulfated and a further rearrangement in crystal compactness takes place because of the expected increase in interlayer spacing due to relatively bulky sulfate groups. Similar sulfation also occurs in the amorphous regions. This change in orientation and the simultaneous breakdown in molecular weight or degree of polymerization leads to an earlier onset of fusion in nanocellulose compared to the cellulose ones. The still narrower width of the fusion endotherm with respect to the cellulose may be attributed to the sulfation effect influencing the increasing proportion of amorphous region also. The acid hydrolysis has led to a breakdown in molecular chain

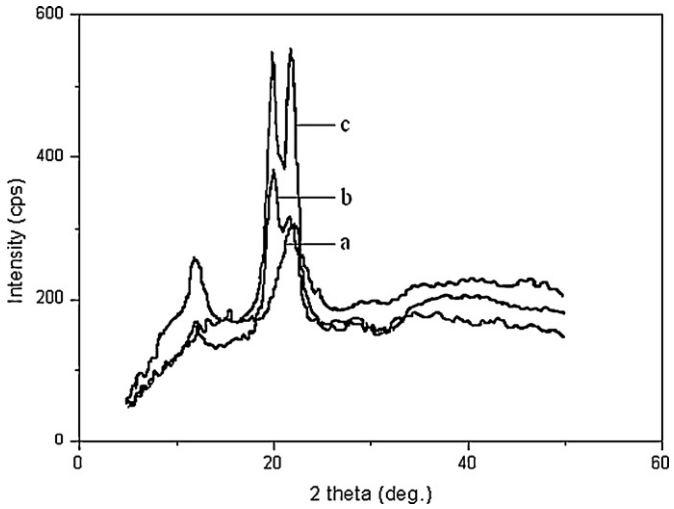

Fig. 4. X-ray diffraction patterns for (a) untreated sugarcane bagasse; (b) alkali treated bagasse, i.e., cellulose; and (c) acid hydrolyzed cellulose, i.e., nanocellulose.

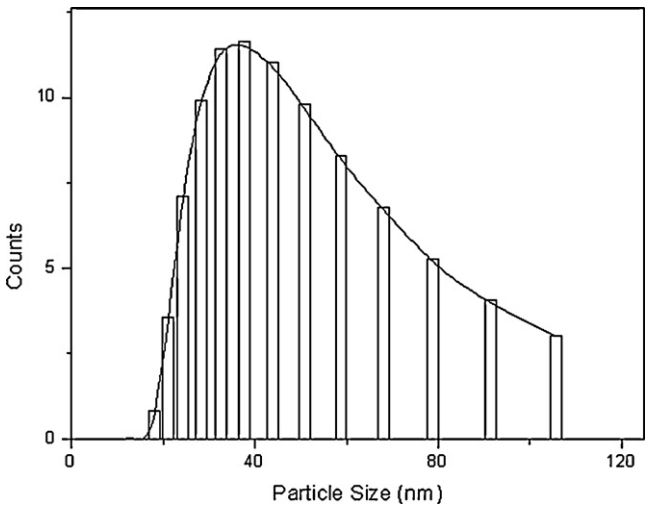

Fig. 5. Particle size distribution of nanocellulose from DLS studies.

length possibly by hydrolyzing the pyranosyl linkages and thus forming small length of crystallites.

4.4. X-ray diffraction studies

The crystallinity of sugarcane bagasse, cellulose and nanocellulose has been analyzed by X-ray diffractometry. It can be noted from Fig. 4 that the fibers show increasing orientation along a particular axis as the non cellulosic polysaccharides are removed and the amorphous zones are dissolved.

All the three diffractograms display two well-defined peaks around $2\theta = 12.5^\circ$ (for 1 1 0 plane) and $2\theta = 22.5^\circ$ (for 2 0 0 plane) characteristic of cellulose (Klemm et al., 2005).

The crystallinity (I_c) was determined by means of Eq. (1) using the height of 2 0 0 peak ($I_{2\,0\,0}$, $2\theta = 22.5^\circ$) and the minimum between the 2 0 0 and 1 1 0 peaks (I_{am}, $2\theta = 18^\circ$). $I_{2\,0\,0}$ represents both crystalline and amorphous material while I_{am} represents amorphous material.

$$I_c = \left[\frac{I_{2\,0\,0} - I_{am}}{I_{2\,0\,0}}\right] \times 100 \quad (1)$$

The percent crystallinity thus goes on increasing in going from the sugarcane bagasse to cellulose and subsequently to nanocellulose. The increase in crystallinity after acid treatment was also observed (Azizi-Samir et al., 2004; Tang et al., 1996).

It is interesting to note that the nanocellulose in the present case shows doublet in the intensity of the main peaks corroborating the

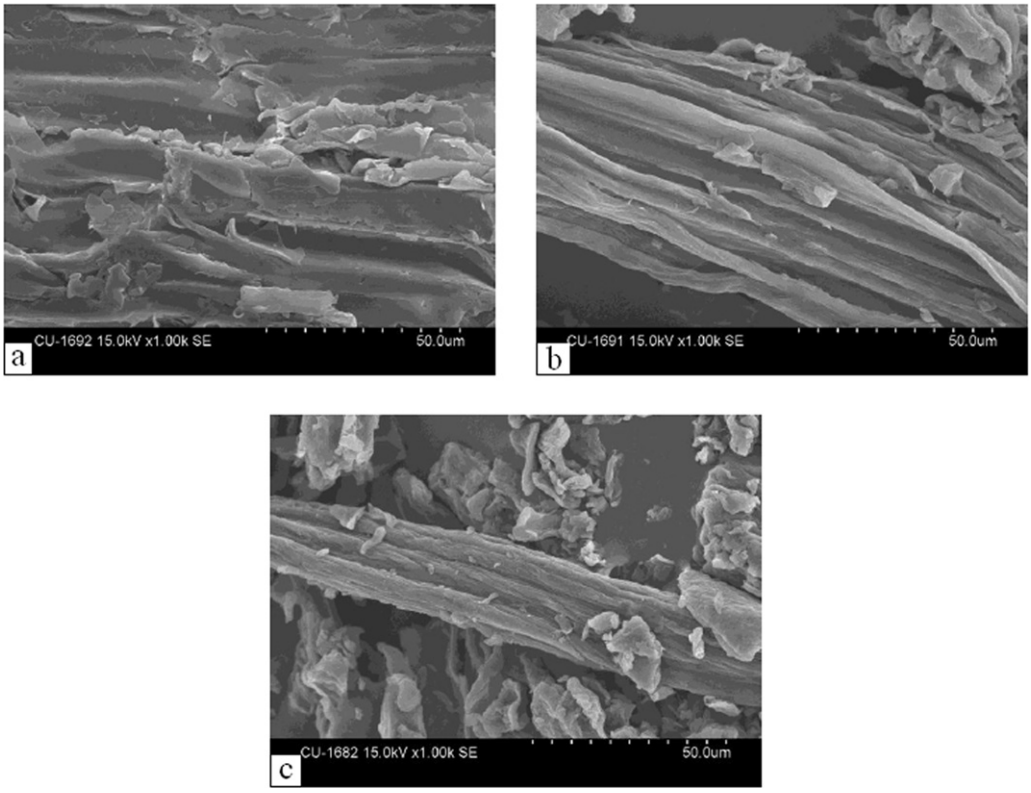

Fig. 6. Scanning electron micrograph of (a) untreated sugarcane bagasse; (b) alkali treated bagasse, i.e., cellulose; and (c) acid hydrolyzed cellulose, i.e., nanocellulose.

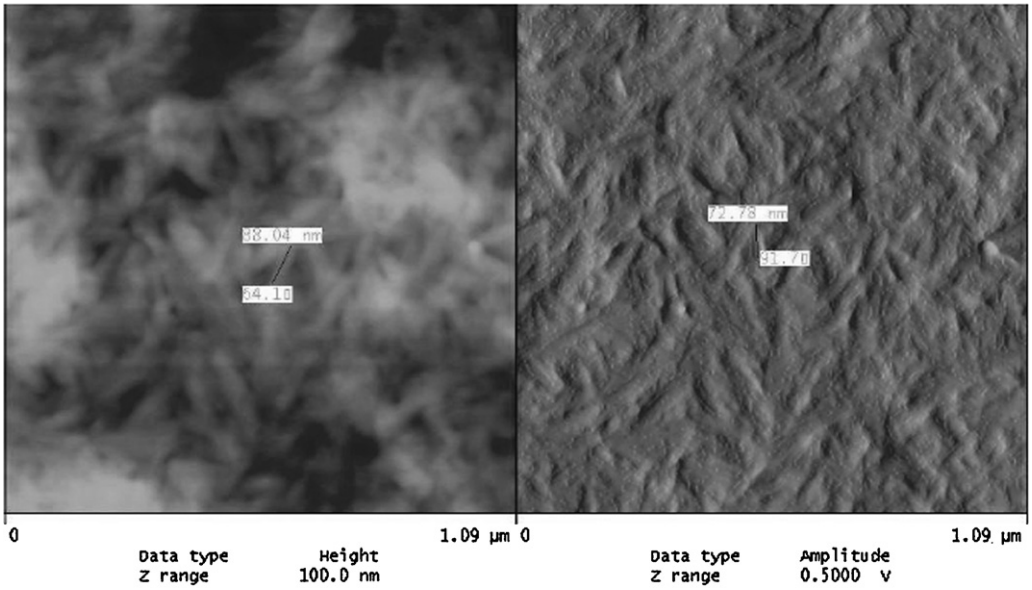

Fig. 7. Atomic force microscopic image of nanocellulose isolated from bagasse.

coexistence of cellulose I and cellulose II allomorphs almost to the same extent ($I_{22.5}/I_{20} \sim 0.93$). The increase of the said ratio may be interpreted as an increase in the proportion of cellulose I crystallites with respect to cellulose II crystallites.

4.5. Particle size distribution of nanocellulose from DLS studies

The DLS technique has been employed to find the statistical distribution of the particles present in nanocellulose, synthesized by the technique as discussed earlier. The statistical distribution as shown in Fig. 5 clearly depicts that the nanocellulose contains majority of the particles lying in the nanorange. The minimum particle size is found to be only 18.17 nm which accounts for only 0.8 volume percent of the nanocellulose under study. There has been a gradual and steady increase in the size of the particles which reaches a peak at 32.84 nm accounting for about 11.5% volume fraction beyond which the rest of the volume fraction has particle sizes greater than 37.84 nm and extent up to about 220 nm accounting for only 0.7% volume fraction. This Maxwell distribution stands as an evidence of nanocellulose synthesis as more than 90% of the volume fraction of particles lies in the nanometric range.

4.6. Morphological and structural characterization

4.6.1. Scanning electron microscopy (SEM) analysis

Fig. 6 shows that the SEM micrographs of the original ground sugarcane bagasse (a), the pure cellulose after the removal of lignin and hemicellulose (b) and finally the nanocellulose produced by acid hydrolysis of the pure cellulose (c).

The diameter of the original sugarcane bagasse fiber was much bigger and each fiber appears to be composed of several microfibrils. Each elementary fiber possesses a compact structure; exhibiting an alignment in the fiber axis direction. The micrograph of the original sugarcane bagasse also displays lot of non-fibrous components scattered over the fiber surface. The overall surface of the fiber is found to be somewhat smooth due to the presence of waxes and oil.

On treating firstly with sodium chlorite the lignin is removed through complex formation and depolymerization. On subsequent treatment with alkali the hemicellulose is hydrolyzed and becomes water soluble. These help in defibrillation of the fibrils and result in micrograph (b) whereby the diameter of the fibrils is reduced to a great extent, also possibly because of removal of non-cellulosic constituents.

Refinement of the fibrillar structure associated with further reduction in its diameter and intermittent breakdown in fibrillar structure in its axial direction are the relevant features in the micrograph of nanocellulose as shown in (c).

4.6.2. Atomic force microscopy (AFM)

In the cellulose fibers, it has been reported (Azizi-Samir et al., 2005) that the sulfuric acid hydrolysis usually could cleave the amorphous region of microfibrils longitudinally, resulting in a diameter reduction of fibers from micron to nanometers. Fig. 7 shows the AFM image of a dilute suspension of cellulose fibers prepared by the treatment of alkali treated sugarcane bagasse with sulfuric acid solution. At least two modes are used to record data during scanning, one for the height image (left-hand image) and the other for the amplitude image (right-hand image). The height image displays topographical detail by tracking the surface with the probe and the amplitude image gives the contrast between soft and hard polymer segments. It is obvious from both the height and the amplitude images that the cellulose obtained after acid hydrolysis under the present experimental set up contains particles and rods in the nano dimension mostly in the range of 70–90 nm.

However, the bright regions represent the crystalline areas while the dark areas stand for the amorphous portions in the direction of the fiber axis in the cellulose structure.

4.6.3. Transmission electron microscopy (TEM)

Fig. 8 shows the TEM micrograph of a very dilute suspension of nanocellulose from sugarcane bagasse. Here it can be seen that the cellulose rods are agglomerated in some places while in some other places they are separated. The distribution range is found to be very long but the majority of the overall size lies in the nanometric range. In Fig. 8 the exact dimension of an elongated cellulose rod has been indicated as 170 nm × 35 nm. Here most of the rods are found to be nanometric in its diameter. The aspect ratio of the rods consequently will be too high.

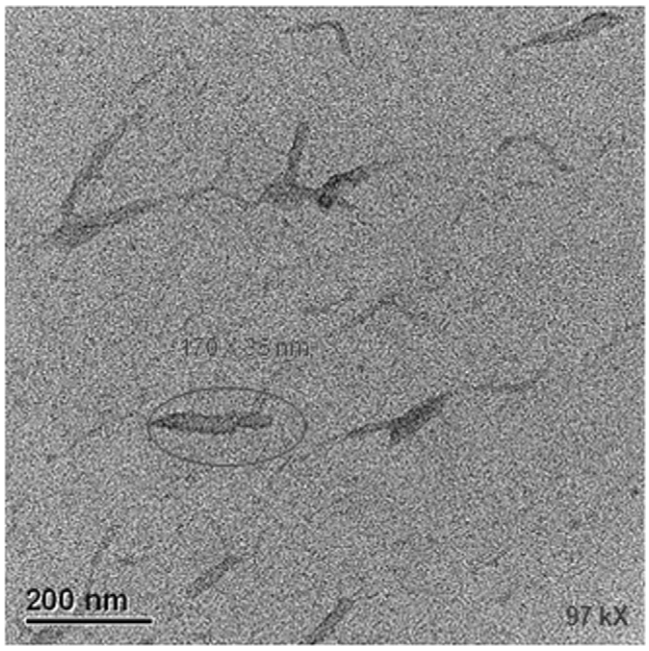

Fig. 8. Transmission electron micrograph from a dilute suspension of nanocellulose.

5. Conclusions

Nanocellulose with a reasonable content of cellulose II has been synthesized from waste sugarcane bagasse. It has been obtained in the form of a stable dispersion where the surface anionic charges help to bring forth the necessary stabilization of the nanocellulose. The AFM studies have given supporting evidence for the formation of nanocellulose. This observation has further been corroborated by the DLS studies which indicate that majority of the hydrolyzed particles lie in the nano range.

Acknowledgements

We hereby acknowledge the assistance from The Calcutta University for its help by the way of research fellowship from the project "Nanoscience and Nanotechnology" and various other infrastructures required for the research work.

References

Araki, J., Wada, M., Kuga, S., & Okano, T. (2000). Birefringent glassy phase of a cellulose microcrystal suspension. *Langmuir*, *16*(6), 2413–2415.
Azizi-Samir, M. A. S., Alloin, F., & Dufresne, A. (2005). Review of recent research into cellulosic whiskers, their properties and their application in nanocomposite field. *Biomacromolecules*, *6*, 612–626.
Azizi-Samir, M. A. S., Alloin, F., Paillet, M., Dufresne, A., et al. (2004). Tangling effect in fibrillated cellulose reinforced nanocomposites. *Macromolecules*, *37*, 4313–4316.
Bondeson, D., Mathew, A., & Oksman, K. (2006). Optimization of the isolation of nanocrystals from microcrystalline cellulose by acid hydrolysis. *Cellulose*, *13*(2), 171–180.
Cherian, B. M., Leão, A. L., de Souza, S. F., Thomas, S., Pothan, L. A., & Kottaisamy, M. (2010). Isolation of nanocellulose from pineapple leaf fibres by steam explosion. *Carbohydrate Polymers*, *81*, 720–725.
Dong, X. M., Revol, J.-F., & Gray, D. G. (1998). Effect of microcrystallite preparation conditions on the formation of colloid crystals of cellulose. *Cellulose*, *5*(1), 19–32.
Dufresne, A. (2006). Comparing the mechanical properties of high performances polymer nanocomposites from biological sources. *Journal of Nanoscience and Nanotechnology*, *6*, 322–330.
Dufresne, A. (2008). Polysaccharide nano crystal reinforced nanocomposites. *Canadian Journal of Chemistry-Revue Canadienne de Chimie*, *86*, 484–494.
Edgar, C. D., & Gray, D. G. (2002). Influence of dextran on the phase behavior of suspensions of cellulose nanocrystals. *Macromolecules*, *35*(19), 7400–7406.
El-sakhawy, M., & Hassan, M. L. (2007). Physical and mechanical properties of microcrystalline cellulose prepared from agricultural residues. *Carbohydrate Polymers*, *67*(1), 1–10.
Fengel, D., & Wegner, G. (1989). *Wood-chemistry, ultrastructure, reactions*. Berlin, New York: Walter de Gruyter.
Garside, P., & Wyeth, P. (2003). Identification of cellulosic fibres by FTIR spectroscopy: Thread and single fibre analysis by attenuated total reflectance. *Studies in Conservation*, *48*(4), 269–275.
Goodger, E. M. (1976). *Hydrocarbon fuels, production, properties and performance of liquids and gases*. London: Macmillan.
Grunert, M., & Winter, W. T. (2000). Progress in the development of cellulose reinforced nanocomposites. *Polymeric Materials Science and Engineering*, *82*, 232.
Grunert, M., & Winter, W. T. (2002). Nanocomposites of cellulose acetate butyrate reinforced with cellulose nanocrystals. *Journal of Polymers and the Environment*, *10*(1/2), 27–30.
Heux, L., Chauve, G., & Bonini, C. (2000). Nonflocculating and chiral-nematic self-ordering of cellulose microcrystals suspensions in nonpolar solvents. *Langmuir*, *16*(21), 8210–8212.
Jacobsen, S. E., & Wyman, C. E. (2002). *Industrial and Engineering Chemistry Research*, *41*, 1454.
Janovsky, A. C., McCredia, E. J., & Janet, E. (2005). *US Patent 5 427 830*;
Janovsky, A. C., McCredia, E. J., & Janet, E. (2005). *Chemical Abstract*, *123*, 114360 z.
Julien, S., Chornet, E., & Overend, R. P. (1993). Influence of acid pre-treatment (H_2SO_4, HCl, HNO_3) on reaction selectivity in the vacuum pyrolysis of cellulose. *Journal of Analytical and Applied Pyrolysis*, *27*, 25–43.
Kadla, J. F., & Gilbert, R. D. (2000). *Cellulose Chemistry and Technology*, *34*, 197.
Khalil, H. P. A., Ismail, H., Rozman, H. D., Ahmad, M. N., et al. (2001). The effect of acetylation on interfacial shear strength between plant fiber and various matrices. *European Polymer Journal*, *37*(5), 1037–1045.
Kim, D. Y., Nishiyama, Y., Wada, M., & Kuga, S. (2001). High-yield carbonization of cellulose by sulphuric acid impregnation. *Cellulose*, *8*, 29–33.
Klemm, D., Heublein, B., Fink, H. P., & Bohn, A. (2005). Cellulose: Fascinating biopolymer and sustainable raw material. *Angewandte Chemie-International Edition*, *44*, 3358–3393.
Lennholm, H., & Iversen, T. (1995). *Nordic Pulp & Paper Research Journal*, *10*, 104.
Lima, M. M. D., & Borsali, R. (2004). Rodlike cellulose microcrystals: Structure, properties, and applications. *Macromolecular Rapid Communications*, *25*, 771–787.
Marchessault, R. H., Morehead, F. F., & Koch, M. J. (1961). Some hydrodynamic properties of neutral suspensions of cellulose crystallites as related to size and shape. *Journal of Colloid Science*, *16*, 327–344.
Marchessault, R. H., Morehead, F. F., & Walter, N. M. (1959). Liquid crystal systems from fibrillar polysaccharides. *Nature*, *184*(9), 632–633.
Maren, R., & William, T. W. (2004). Effect of sulfate groups from sulfuric acid hydrolysis on the thermal degradation behavior of bacterial cellulose. *Biomacromolecules*, *5*, 1671–1677.
Nacos, M., Katapodis, P., Pappas, C., Daferera, D., Tarantilis, P. A., Christakopoulos, P., et al. (2006). Kenaf xylan—A source of biologically active acidic oligosaccharides. *Carbohydrate Polymers*, *66*(1), 126–134.
Nguyen, T., Zavarin, E., & Barrall, E. M. (1981). Thermal-analysis of lignocellulosic materials. Part 1: Unmodified materials. *Journal of Macromolecular Science, Part C: Polymer Reviews*, *20*, 1–65.
Nickerson, R. F., & Habrle, J. A. (1947). *Industrial and Engineering Chemistry*, *39*, 1507.
Nishino, T., Takano, K., & Nakamae, K. J. (1995). *Polymer Science B*, *33*, 1647.
Norman, A. G., & Jenkins, S. H. (1933). A new method for the determination of cellulose, based upon observations on the removal of lignin and other encrusting materials. *Biochemical Journal*, *27*, 818–831.
Oksmann, K., & Sain, M. (2006). *Cellulose nanocomposites-processing, characterization and properties*. Washington, DC: American Chemical Society.
Ono, S., & Keiko, K. (1995). Kokai Tokkya Koho. *JP Patent 07 143 856*;
Ono, S., & Keiko, K. (1995). *Chemical Abstract*, *123*, 197252 w.
Orts, W. J., Godbout, L., Marchessault, R. H., & Revol, J.-F. (1998). Enhanced ordering of liquid crystalline suspensions of cellulose microfibrils: A small-angle neutron scattering study. *Macromolecules*, *31*(17), 5717–5725.
Pandey, A., Soccol, C. R., Nigam, P., & Soccol, V. T. (2000). Biotechnological potential of agro-industrial residues I: Sugarcane bagasse. *Bioresource Technology*, *74*(1), 69–80.
Panosyan, I., Skurikhin, I. I., Sviridov, A. F., & Kiseleva, T. (1994). *Voprosy Pitaniia*, *4*, 45;
Panosyan, I., Skurikhin, I. I., Sviridov, A. F., & Kiseleva, T. (1995). *Chemical Abstract*, *123*, 226191 h.
Pappas, C., Tarantilis, P. A., Daliani, I., Mavromoustakos, T., & Polissiou, M. (1999). *Ultrasonics Sonochemistry*, *5*, 163.
Pu, Y. Q., Zhang, J. G., Elder, T., Deng, Y., Gatenholm, P., Ragauskas, A., et al. (2007). Investigation into nanocellulosics versus acacia reinforced acrylic films. *Composites Part B: Engineering*, *38*, 360–366.
Ranby, B. G. (1952). *Tappi*, *35*, 53.
Revol, J. F., Godbout, L., Dong, X. M., Gray, D. G., Chanzy, H., & Maret, G. (1994). Chiral nematic suspensions of cellulose crystallites; phase separation and magnetic field orientation. *Liquid Crystals*, *16*(1), 127–134.
Ristolainen, M., Alen, R., Malkavaara, P., & Pere, J. (2002). *Holzforschung*, *56*, 513.
Rozmarin, G. H., Ungureanu, V., Stoleru, A., et al. (1977). A study on the supramolecular structure of cellulose carried out by means of acid hydrolysis. *Cellulose Chemistry and Technology*, *11*, 523–530.
Sain, M., & Panthapulakkal, S. (2006). Bioprocess preparation of wheat straw fibers and their characterization. *Industrial Crops and Products*, *23*, 1–8.
Sidiras, D. K., & Koukios, E. G. (1989). Acid saccharification of ball-milled straw. *Biomass*, *19*(4), 289–306.
Simkovic, I., Mlynar, J., & Alfoldi, J. (1990). *Holzforschung*, *44*, 113.

Song, S. K., & Lee, Y. Y. (1984). Acid hydrolysis of wood cellulose under low water condition. *Biomass*, *6*(1–2), 93–100.
Sun, J. X., Sun, X. F., Zhao, H., & Sun, R. C. (2004). Isolation and characterization of cellulose from sugarcane bagasse. *Polymer Degradation and Stability*, *84*(2), 331–339.
Sun, X. F., Xu, F., Sun, R. C., Fowler, P., & Baird, M. S. (2005). Characteristics of degraded cellulose obtained from steam-exploded wheat straw. *Carbohydrate Research*, *340*, 97–106.
Tang, L. G., Hon, D. N. S., Pan, S. H., Zhu, Y. Q., Wang, Z., & Wang, Z. Z. (1996). Evaluation of microcrystalline cellulose. I. Changes in ultrastructural characteristics during preliminary acid hydrolysis. *Journal of Applied Polymer Science*, *59*, 483–488.
Teixeira, E. M., Pasquini, D., Curvelo, A. A. S., Corradini, E., Belgacem, M. N., Dufresne, A., et al. (2009). Cassava bagasse cellulose nanofibrils reinforced thermoplastic cassava starch. *Carbohydrate Polymers*, *78*, 422–431.
Troedec, M., Sedan, D., Peyratout, C., Bonnet, J., Smith, A., Guinebretiere, R., et al. (2008). Influence of various chemical treatments on the composition and structure of hemp fibers. *Composites Part A-Applied Science and Manufacturing*, *39*(3), 514–522.
Wang, W. M., Cai, Z. S., Yu, J. Y., Xai, Z. P., et al. (2009). Changes in composition, structure, and properties of jute fibers after chemical treatments. *Fibers and Polymers*, *10*(6), 776–780.
Wyman, C. E. (1999). *Annual Review of Energy and the Environment*, *24*, 189.
Yao, S. J. (1999). Sulfation kinetics in the preparation of cellulose sulphate. *Chinese Journal of Chemical Engineering*, *7*, 47–55.
Zhang, J., Jiang, N., Dang, Z., Elder, T. J., & Ragauska, A. J. (2008). Oxidation and sulfonation of cellulosics. *Cellulose*, *15*, 489–496.
Zimmerman, T., Pöhler, E., & Schwaller, P. (2005). *Advanced Engineering Materials*, *12*, 1156.